

MICROCOPY RESOLUTION TEST CHART
NATIONAL BUREAU OF STANDARDS-1963-A

LEVEL

12
P.S.

ADA 081 797

6 A HIGHER ORDER SURFACE SINGULARITY METHOD FOR THE AXISYMMETRIC INVERSE PROBLEM.

10 J. Fernandez

12 44

DTIC ELECTE
MAR 14 1980

Technical Memorandum
File No. TM 79-125
June 25, 1979
Contract No. N00024-79-C-6043
Copy No. 27

9/T

The Pennsylvania State University
APPLIED RESEARCH LABORATORY
Post Office Box 30
State College, PA 16801

Page 25 Jun 79
G.../TM-79-125

DDC FILE COPY

Approved for Public Release
Distribution Unlimited

NAVY DEPARTMENT
NAVAL SEA SYSTEMS COMMAND

79 12 18 36

11007

JCL

UNCLASSIFIED

SECURITY CLASSIFICATION OF THIS PAGE (When Data Entered)

REPORT DOCUMENTATION PAGE		READ INSTRUCTIONS BEFORE COMPLETING FORM
1. REPORT NUMBER TM 79-125	2. GOVT ACCESSION NO.	3. RECIPIENT'S CATALOG NUMBER
4. TITLE (and Subtitle) A HIGHER ORDER SURFACE SINGULARITY METHOD FOR THE AXISYMMETRIC INVERSE PROBLEM		5. TYPE OF REPORT & PERIOD COVERED Technical Memorandum
		6. PERFORMING ORG. REPORT NUMBER
7. AUTHOR(s) J. Fernandez		8. CONTRACT OR GRANT NUMBER(s) N00024-79-C-6043
9. PERFORMING ORGANIZATION NAME AND ADDRESS Applied Research Laboratory ✓ P. O. Box 30 State College, PA 16801		10. PROGRAM ELEMENT, PROJECT, TASK AREA & WORK UNIT NUMBERS
11. CONTROLLING OFFICE NAME AND ADDRESS Naval Sea Systems Command - Code NSEA-63R-31 Department of the Navy Washington, DC 20362		12. REPORT DATE June 25, 1979
		13. NUMBER OF PAGES 37
14. MONITORING AGENCY NAME & ADDRESS (if different from Controlling Office)		15. SECURITY CLASS. (of this report) UNCLASSIFIED
		15a. DECLASSIFICATION/DOWNGRADING SCHEDULE
16. DISTRIBUTION STATEMENT (of this Report) Approved for Public Release. Distribution Unlimited. Per NAVSEA - July 31, 1979		
17. DISTRIBUTION STATEMENT (of the abstract entered in Block 20, if different from Report)		
18. SUPPLEMENTARY NOTES hydrodynamics, singularity		
19. KEY WORDS (Continue on reverse side if necessary and identify by block number)		
20. ABSTRACT (Continue on reverse side if necessary and identify by block number) The hydrodynamic design of an axisymmetric body with certain performance characteristics requires the solution to the inverse problem wherein the pressure distribution on the body is specified and the corresponding body profile must be determined. This paper presents an efficient inverse method for incompressible, axisymmetric potential flows employing a higher order surface singularity technique with parabolic surface elements and linearly varying sources. The body shape is obtained through an iterative		

DD FORM 1 JAN 73 1473

EDITION OF 1 NOV 65 IS OBSOLETE

UNCLASSIFIED

SECURITY CLASSIFICATION OF THIS PAGE (When Data Entered)

UNCLASSIFIED

SECURITY CLASSIFICATION OF THIS PAGE(When Data Entered)

↙
scheme using the stream function to predict the body profile. The method is rapidly convergent and shows excellent agreement in cases where solutions are known. ↘

UNCLASSIFIED

SECURITY CLASSIFICATION OF THIS PAGE(When Data Entered)

Accession For	
DTIC GRA&I	<input checked="" type="checkbox"/>
DDC TAB	<input type="checkbox"/>
Unannounced	<input type="checkbox"/>
Justification	<input type="checkbox"/>
By _____	
Distribution/	
Availability Codes	
Dist	Availand/or special

Subject: A Higher Order Surface Singularity Method for the Axisymmetric Inverse Problem

References: See Page 29

Abstract: The hydrodynamic design of an axisymmetric body with certain performance characteristics requires the solution to the inverse problem wherein the pressure distribution on the body is specified and the corresponding body profile must be determined. This paper presents an efficient inverse method for incompressible, axisymmetric potential flows employing a higher order surface singularity technique with parabolic surface elements and linearly varying sources. The body shape is obtained through an iterative scheme using the stream function to predict the body profile. The method is rapidly convergent and shows excellent agreement in cases where solutions are known.

Acknowledgment: The author wishes to thank Drs. B. R. Parkin and G. H. Hoffman for their encouragement and interest in the progress of this work. This work was supported by the U. S. Naval Sea Systems Command, Code NSEA-63R-31.

Table of Contents

	<u>Page</u>
Abstract	1
Acknowledgment	1
List of Figures	3
Nomenclature	4
I. INTRODUCTION	6
1.1 Aim	6
1.2 Earlier Studies	7
1.3 Present Study	8
II. PROBLEM FORMULATION AND THE METHOD OF SOLUTION	10
2.1 Body Geometry	10
2.2 Source Distribution	11
2.3 Surface Integrals	12
2.4 The Influence Coefficients	14
2.5 The Conditions on the Body	16
2.6 The Iterative Solution	17
III. RESULTS AND CONCLUSIONS	19
APPENDIX: Stream Function for a Source Ring in Unbounded Medium	23
References	29
Figures	32

List of Figures

<u>Figure</u>	<u>Title</u>	<u>Page</u>
1	Element Geometry	32
2	Algorithm for the Inverse Method	33
3	Successive Iterations for the Modified Spheroid	34
4	Low-Drag Cusped Body	35
5	Roof-Top Pressure Distribution	36
6	Equivalent Bodies	37

Nomenclature

A	influence coefficient matrix
B	array of closure coefficients
C	element semi-curvature
E(m)	complete elliptic integral of the second kind
$F_1(s,s')$	axial velocity at s due to a unit source at s'
$F_2(s,s')$	radial velocity at s due to a unit source at s'
$F_3(s,s')$	stream function at s due to a unit source at s'
$J_n(x)$	Bessel function of the first kind and order n
K(m)	complete elliptic integral of the first kind
l	total arc length of the body along the meridian
m	modulus of the elliptic integrals
N	number of surface elements
P	field point or observation point
P'	source point
r	radius
s	arc length parameter
z	axial distance
α	angle between z-axis and the normal to the body pointing into the fluid
δ	tolerance parameter for surface velocity
Δ	element base length
η	ordinate of the element's local co-ordinate system
ϕ	velocity potential

Nomenclature (continued)

σ	source strength
ψ	stream function
θ	element slope

I. Introduction

1.1 Aim:

The hydrodynamic design of an axisymmetric body with certain performance characteristics requires the solution of the inverse problem wherein the pressure distribution on the body is specified and the corresponding body profile must be determined. It is well-known that the skin friction distribution on the body is related to the pressure distribution for non-separating flows. Thus, the inverse problem arises in the search for low-drag body shapes. The solution to the inverse problem in two-dimensional plane flow has been known for many years. This solution is fairly straightforward and is obtained by conformal mapping techniques. Such simple mapping techniques are not possible for axisymmetric flows because the axisymmetric Laplace's equation is not invariant under conformal mapping. Many early investigations of the axisymmetric inverse problem have yielded unsatisfactory results and only recently have successful methods been developed [1, 2, 3]. These methods which are essentially numerical use the solution to the direct problem in an iterative manner. These iterative methods are either slowly convergent [1] or applicable only to simple body shapes [2,3]. The present effort was, therefore, undertaken in order to develop an efficient inverse method which is rapidly convergent and is applicable to arbitrary axisymmetric bodies.

1.2 Earlier Studies:

One of the early investigations of the axisymmetric inverse problem was by Young and Owen [4], employing axial source distributions. Their theory assumed that the perturbation velocities are small compared to the free stream velocity and thus is applicable only to slender bodies of revolution. Their method is essentially the same as that of the slender body theory which evolved subsequent to their work. A later method due to McKnown and Hsu [5] turned out to be the same as the Young and Owen method. A subproblem to the inverse problem was solved by Marshall [6]. In this subproblem, which Marshall called the "development problem," a small change in body shape is obtained for a specified small change in pressure distribution. An interesting class of inverse problem is the cavitation problem which requires the cavity shape for a given cavitation number. In this case, the pressure distribution remains constant. Such cavity problems for axisymmetric flows have been treated by Munzer and Reichardt [7], Garabedian [8], and Jeppson [9].

Among the recent axisymmetric inverse techniques is the method due to James [10] who used a mapping function involving series expansion. His results are applicable only for bodies with blunt or cusped tails. For the case of bodies whose tail shapes are neither blunt nor cusped, James' method requires a mapping function involving fractional powers but he did not consider this case. The two recent methods that are successful are due to Bristow [1] and Zedan and Dalton [2,3]. These methods start with an initial guess of the body shape and use a variant of the direct problem solution in an iterative manner in order

to update the body geometry. Bristow's method uses the Douglas-Neumann direct method in which the body surface is discretized into conical elements and the source strength remains constant over each surface element. Zedan and Dalton use axial sources for their analysis. Their earlier work [2] employed axial source elements with constant source strengths while their later work [3] uses linearly varying source strengths on each axial element.

1.3 Present Study:

In the present study we employ a higher order surface singularity method for the solution of the axisymmetric inverse problem. In this method the body surface is discretized into paraboloidal elements. The source strength on each element is taken as linearly varying so that the formulation remains consistent [11]. The present method starts with an initial body profile which is an ellipse or a parabola of reasonable fineness. The tangential velocity on the body is obtained from the prescribed pressure distribution by using the Bernoulli equation. The tangential velocity distribution along with the body closure condition are used to obtain the source strength distribution on the body. The improved shape is now given by the shape of the zero streamline. The initial shape is replaced by the improved shape and the computation is continued iteratively until the body shape converges. Usually convergence is obtained in four iterations. The use of the stream function to predict the improved body shape is similar to the technique used by Zedan and Dalton [2,3]. However, Zedan and Dalton use axial singularities and their method cannot handle bodies with

June 25, 1979

JF:mmj

sharp corners or sudden changes in slope. The present method employs surface sources and, therefore, is capable of dealing with axisymmetric bodies of arbitrary shapes. In comparison with Bristow's method [1], the present method (i) uses higher order surface elements as well as higher order source distributions, and (ii) employs an improved algorithm for the body shape prediction. These improvements result in faster convergence. The present method converges in four iterations while Bristow's method converges in ten iterations.

II. Problem Formulation and the Method of Solution

2.1 Body Geometry:

Consider an axisymmetric body placed in an unbounded free stream at zero angle of attack. Let the body profile be approximated by N parabolic elements whose end points are given by the sequence $\{(z_{2j-1}, r_{2j-1}), 1 \leq j \leq N + 1\}$. The shape of the j -th element can then be represented by the parabola

$$\eta = C_j (\xi^2 - \Delta_j^2/4) \tag{1}$$

where (ξ, η) is a coordinate system local to each element such that the ξ axis passes through the end points of the element and the η axis is the perpendicular bisector of the element chord. The length of the chord is Δ_j while C_j is the element curvature. The slope θ_j of the element is taken as the slope of its chord (Figure 1). In general, the curvature C_j for each element is taken as the geometric mean of the curvatures of the two parabolas, the left parabola passing through the end points of the elements j and $j-1$, while the right parabola passes through the end points of the elements j and $j+1$. If the two curvatures are of different signs then C_j is taken as zero. The curvature C_{jL} of the left parabola is given by

$$C_{jL} = \frac{-\tan(\theta_{j-1} - \theta_j)}{\Delta_j + \Delta_{j-1} \cos(\theta_{j-1} - \theta_j)} \tag{2.1}$$

while the curvature C_{jR} of the right parabola is given by

$$C_{jR} = \frac{-\tan(\theta_j - \theta_{j+1})}{\Delta_j + \Delta_{j+1} \cos(\theta_j - \theta_{j+1})} \quad (2.2)$$

For the first element we take $C_1 = C_{1R}$ while for the last element $C_N = C_{NR}$. The boundary conditions of zero normal velocity and the prescribed tangential velocity are to be applied at the mid-points of the element arcs. These points correspond to $\xi = 0$ for each surface element. The sequence of points where the boundary conditions are applied are called control points and are denoted by $\{(z_{2j}, r_{2j}), 1 \leq j \leq N\}$. The locations of the control points are calculable from the specified end points and the element geometry.

2.2 Source Distribution:

It is well-known that the flow around the body can be represented by a source distribution over its surface. Since the flow field is axisymmetric, the source distribution will consist of source rings. For the parabolic representation of body elements, the source distribution on each element must vary linearly so that the formulation remains consistent [11]. The source distribution for the j -th element is then given by

$$\sigma(\xi) = \frac{(\sigma_j + \sigma_{j+1})}{2} + \frac{(\sigma_{j+1} - \sigma_j)}{\Delta_j} \xi, \quad -\frac{\Delta_j}{2} \leq \xi \leq \frac{\Delta_j}{2} \quad (3)$$

The unknowns $\sigma_1, \dots, \sigma_{N+1}$ are the source strengths at the $N + 1$ end points of the elements. Equation (3) ensures that the source

distribution is continuous over the body surface and is linearly varying across each element. From the source distribution and the body geometry, the velocity potential and the stream function at any point can be obtained. For the purpose of our analysis, we shall employ the notation whereby the source point is denoted by a primed entity while the field point (or the observation point) is denoted by an unprimed entity.

2.3 Surface Integrals:

The condition of zero normal velocity on the body is given by [12]

$$h(s) = -\frac{1}{2} \sigma(s) + \int_0^{\ell} \sigma(s') [F_1(s, s') \cos \alpha + F_2(s, s') \sin \alpha] r' ds' \quad (4)$$

where the parameter s is the arc length at any point on the body along its meridian, ℓ is the total arc length of the body, $h(s)$ is the component of the free stream along the inward normal to the body, and α is the angle between the z -axis and the outward normal to the body. The influence functions F_1 and F_2 are related to the velocity potential ϕ by [12]

$$\left. \begin{aligned} F_1(s, s') &= 2\pi \frac{\partial \phi}{\partial z} (z, r; z', r') \\ F_2(s, s') &= 2\pi \frac{\partial \phi}{\partial r} (z, r; z', r') \end{aligned} \right\} \quad (5)$$

It should be noted that the coordinates (z, r) on the body in Equation (5) are functions of the arc length s .

The tangential velocity V_T on the body can be obtained from

$$V_T = \sin \alpha - \int_0^l \sigma(s') [F_1(s,s') \sin \alpha - F_2(s,s') \cos \alpha] r' ds' . \quad (6)$$

The first term on the right is the component due to the free stream while the integral represents the contribution from the source distributions.

The stream function at any point s on the body is given by

$$\Psi(s) = \frac{r^2}{2} - \int_0^l \sigma(s') F_3(s,s') r' ds' . \quad (7)$$

The first term on the right hand side of Equation (7) represents the stream function due to the free stream while the second term is due to the source distribution on the body. The influence function F_3 is related to the stream function by

$$F_3(s,s') = 2\pi \psi(s,s') , \quad (8)$$

where $\psi(s,s')$ is the stream function at s due to a unit ring source at s' . In terms of the (z,r) coordinates the three influence functions are given by

$$F_1(s,s') = - \frac{E(m)(z - z')}{\pi(1 - m^2) p^3} , \quad (9)$$

$$F_2(s,s') = - \frac{1}{2\pi r p} \left[\frac{\{r^2 - r'^2 - (z - z')^2\} E(m)}{(r - r')^2 + (z - z')^2} + K(m) \right] , \quad (10)$$

$$F_3(s, s') = \text{Sgn}(z - z') F_3^* \quad (11)$$

where

$$F_3^* = \frac{|z - z'| r K(m)}{\pi p(r + r')} + \frac{1}{4} [1 - \Lambda_0(\epsilon; m)] \quad r \geq r'$$

$$= \frac{|z - z'| r K(m)}{\pi p(r + r')} + \frac{1}{4} [1 + \Lambda_0(\epsilon; m)] \quad r < r' .$$

The functions F_1 and F_2 are derived in Reference [12].

The function F_3 is derived in the Appendix where the functions p , $\Lambda_0(\epsilon; m)$ are also defined.

2.4 The Influence Coefficients:

In the implementation of the inverse method, the surface integrals of functions F_1 , F_2 , and F_3 , indicated by Equations (5 - 7), are discretized over the body. The body radius r' , the source distribution $\sigma(s')$ and the elemental arc ds' are expressed in terms of the local coordinate ξ , and the integration is carried out with respect to ξ for each element. It should be noted that α , the slope of the normal is a function of the observation point s and is, therefore, independent of ξ . In this discretization process the following two forms of integrals arise:

$$x_{ijk}^0 = \int_{-\Delta_j/2}^{\Delta_j/2} F_k(s_i, \xi) r'(\xi) \frac{ds'}{d\xi} d\xi, \quad (12)$$

and

$$X_{ijk}^1 = \int_{-\Delta_j/2}^{\Delta_j/2} F_k(s_i, \xi) r'(\xi) \frac{ds'}{d\xi} \xi d\xi \quad (13)$$

The subscript k can take values 1, 2, or 3. The coefficient X_{ijk}^0 is due to the constant term in Equation (3), while X_{ijk}^1 is due to the first order term in Equation (3). Further, these coefficients are assembled into three $N \times (N+1)$ matrices $\{A_k, 1 \leq k \leq 3\}$ such that element $A_k(i, j)$ is the influence coefficient due to the source strength σ_j at the i -th control point. The contribution of each of the X -coefficients to the appropriate element of matrix A is calculable from Equation (3). In order to minimize the storage requirements for the computer program, the elements of A_k are assembled as each X -coefficient is being generated. The integrals (12) and (13) are evaluated by Simpson's rule and pose no difficulty when $i \neq j$. However, when $i = j$ the integrand in Equation (12) becomes singular for $k = 1, 2$, which occurs when $\xi = 0$. In this case, the interval $-\Delta_j/2 \leq \xi \leq \Delta_j/2$ is divided into three subintervals $-\Delta_j/2 \leq \xi \leq h$, $-h \leq \xi \leq h$, and $h \leq \xi \leq \Delta_j/2$. The integrals over the first and the third subintervals are evaluated by Simpson's rule. The integral over the singular subinterval is evaluated analytically. These analytical results are similar to those of Reference [13] except for the differences due to the respective variables of integration. The function F_3 is non-singular when $i = j$, but has a finite discontinuity

at $\xi = 0$ as shown in the Appendix. In this case the integrals (12) and (13) are obtained by evaluation over the two subintervals $-\Delta_j/2 \leq \xi \leq 0$ and $0 \leq \xi \leq \Delta_j/2$.

2.5 The Conditions on the Body:

The velocity on the body is purely tangential since the normal velocity must be zero. Thus, the tangential velocity, V_T , can be obtained from the prescribed pressure distribution through the Bernoulli equation. The tangential velocity condition, viz. Equation (6), can then be discretized as

$$\sum_{j=1}^{N+1} [A_1(i,j) \cos \alpha_i + A_2(i,j) \sin \alpha_i] \sigma_j = \cos \alpha_i - V_{Ti} \quad , \quad (14)$$

where A_1, A_2 are the influence coefficient matrices and V_{Ti} is the prescribed tangential velocity at i -th control point. The conditions that the normal velocity on the body be zero and the value of the stream function on the body remain constant are equivalent.

The later condition is our natural choice since the improved body shape for the iterative process will then be given by the shape of the zero streamline. Thus, the stream surface condition on the body can be written as

$$\sum_{j=1}^{N+1} A_3(i,j) \sigma_j = \frac{r_i^2}{2} \quad , \quad (15)$$

where r_i is the radius of the body at the i -th control point. Finally, in order that the body is closed, the areal sum of sources on the body

should be zero [12]. This is the body closure condition and is given by

$$\int_0^{\ell} \sigma(s') r' ds' = 0 \quad . \quad (16)$$

Introducing the approximations for the source distribution and the body geometry in Equation (16) one obtains integrals similar to those of Equations (12) and (13). In this case the function F_k will, of course, be replaced by unity. Collecting the coefficients of σ_j in this approximation, Equation (16) can be discretized as

$$\sum_{j=1}^{N+1} B(j) \sigma(j) = 0 \quad . \quad (17)$$

The computation of $B(j)$ is similar to that of a row in matrix $A_k(i,j)$.

2.6 The Iterative Solution:

The conditions enumerated in the previous section contain the ingredients for an iterative solution of the inverse problem. The iterative solution starts with an initial guess of the meridian profile of the body. This guess usually is an ellipse or a parabola of reasonable fineness ratio. The matrices A_1 , A_2 , A_3 , and B are then obtained from the initial body geometry. The $(N+1)$ unknown source strengths $\{\sigma_j\}$ are then obtained by solving the tangential velocity conditions given by Equation (14) at the N control points along with the body closure conditions, Equation (17). Equations (14) and (17) are cast into an $(N+1) \times (N+1)$ matrix equation and the unknown $\{\sigma_j\}$ are obtained by the standard Gaussian elimination method. These linear equations are

well conditioned and no difficulties have been encountered in obtaining the source strengths. The improved body shape is now given by $\{r_i\}$, the radii at the control points, which are obtained from Equation (15). These N points along with the body end points constitute the improved body shape. The quantities associated with the element geometry, like the slopes, curvatures, etc., must be obtained by interpolation. In order that the slopes and curvatures vary continuously, the interpolation is carried out by means of cubic splines [14]. The initial body shape is now replaced by the improved shape and the iterative process is continued until convergence is obtained. When the computed tangential velocity for the improved body agrees with the prescribed values within a prescribed tolerance, the iteration is taken as converged. Specifically, the Root Mean Square (RMS) error in velocity, averaged over all the control points, must be less than a given tolerance. Thus, the convergence criterion is

$$\left\{ \frac{1}{N} \sum_{i=1}^N (v_{Ti}^C - v_{Ti}^P)^2 \right\}^{\frac{1}{2}} \leq \delta \quad , \quad (18)$$

where the superscript C refers to calculated values and P refers to prescribed values. The value of δ is usually taken as 10^{-3} . Another possible convergence criterion is to require that the RMS difference in the radii at the control points for two successive iterations be less than a given tolerance. But the convergence in tangential velocity is more reliable and is employed in the computer program. A flow chart for the algorithm used in the inverse method is shown in Figure 2.

III. Results and Conclusions

The present inverse method has been applied to various body shapes of interest in order to test its efficacy. The first test case was a spheroid with a tangent cone at the tail. The shape of this modified spheroid was specified by the equations

$$\begin{aligned} r &= \beta \sqrt{z(\alpha-z)} & , & & 0 \leq z \leq z_0 . \\ &= A(1-z) & , & & z_0 \leq z \leq 1 . \end{aligned} \quad (19.1)$$

The various parameters for this modified spheroid are given by

$$\begin{aligned} \alpha &= 0.96324 & z_0 &= 0.92910 \\ \beta &= 0.16447 & A &= 0.41318 \end{aligned} \quad (19.2)$$

The pressure distribution for this spheroid in unbounded flow was obtained by a direct solution method using the surface singularity technique [12]. This pressure distribution was used as the input to the inverse method. The initial body shape was taken as an ellipsoid of thickness ratio 0.08. The results from the inverse method are shown in Figure 3. It should be noted that the vertical scale has been exaggerated in order to magnify the differences between successive iterations. The shapes obtained in successive iterations are labeled with the corresponding iteration numbers and the initial shape is labeled as zero. With the prescribed tolerances, the present method converges to the exact shape in four iterations.

A low-drag body with cusped tail was taken as the next test case. The shape of this body is specified by the equations

$$\begin{aligned} r &= r_m [-1.1723\zeta_1^4 + 0.7088\zeta_1^3 + 1.0993\zeta_1^2 + 0.3642\zeta_1]^{1/2} , & 0 \leq z \leq z_m \\ &= r_m [-0.11996\zeta_2^5 - 2.58278\zeta_2^4 + 3.52544\zeta_2^3 + 0.1773\zeta_2^2]^{1/2} , & z_m < z \leq 1 . \end{aligned} \quad (20.1)$$

The parameters in the above equation are given by

$$\begin{aligned} \zeta_1 &= z/z_m & \zeta_2 &= (1-z)/(1-z_m) \\ z_m &= 0.4446 & r_m &= 0.117 \end{aligned} \tag{20.2}$$

The pressure distribution corresponding to this shape was obtained by the direct method [12]. The pressure distribution shows a stagnation point at the nose where the pressure drop is rapid, followed by a gradual pressure drop to the minimum pressure point at about 45 percent of the body length. The minimum pressure point also corresponds to the maximum thickness point on the body. The pressure recovery is gradual and there is no stagnation point at the tail because of the cusp. The pressure distribution along with a parabolic initial shape were taken as input to the inverse method. The body was divided into 30 intervals using a cosine distribution so that the intervals are smaller near the nose and the tail. The results obtained are shown in Figure 4 where the solid curve marked "expected shape" corresponds to Equations (20). The circles which correspond to the body shape obtained at the fourth iteration agree very well with the exact shape. A difficulty was encountered during the initial iterations in this case, whereby the value of R^2 became negative near the tail region of the body. The difficulty was overcome by normalizing the body coordinates with respect to the body length corresponding to the point $R = 0$ near the tail.

While the foregoing examples verify the correctness of the inverse method, its usefulness lies in the ability to synthesize bodies corresponding to prescribed pressure distributions. As a start toward this end the inverse method was used to find the body shape for a hypothetical constant pressure distribution. In this case, the pressure drop and recovery are confined

respectively to five percent of the body length fore and aft. Stagnation points exist at the nose and tail where $C_p = 1$. The number of intervals in this case was also 30 with the points selected using a Cosine distribution. Convergence was obtained in four iterations and the body obtained is symmetrical and resembles an ellipsoid (Figure 5). The pressure distribution on the resultant body, computed by the direct method [12] is shown by the circles. The agreement is very good except in the "corner" regions of the prescribed pressure distribution. The computed body tends to smooth the discontinuous slopes of the pressure distribution. Such constant pressure designs are useful in maintaining laminar flow on the body and thus minimizing the drag.

Figure 6 presents two bodies, one in unbounded flow and the other in a cylindrical tunnel, which have the same pressure distribution. In this sense, the two bodies are equivalent. The pressure distribution for a cylindrical body with spherical ends, in a tunnel of infinite length, was obtained by the direct method [12] and is shown in Figure 6. The in-tunnel body is shown by the broken curve in Figure 6. The tunnel diameter and the body length were taken respectively as 6 and $3\frac{1}{2}$ times the body diameter. The pressure drop is rapid near the nose and the tail with the minimum pressure points located at about 12 percent of the body length from the ends of the body. The inverse calculations for this pressure distribution in unbounded flow resulted in a body of greater curvature and thickness than the body in-tunnel. This behavior is caused by the increased surface velocities on the body in-tunnel. This calculation employed 50 intervals and convergence was obtained in four iterations. This type of analysis is of interest in relating water/wind tunnel tests to performance in an unbounded medium.

The foregoing results demonstrate that the present inverse method shows excellent agreement in cases where the results are known. The method is also rapidly convergent. In combination with a drag estimation technique, the inverse method can be used for obtaining low-drag body shapes. The method is currently being applied to a family of pressure distributions in a parametric-design study. In conjunction with the results of Reference [12], the present method is capable of being extended to the inverse problem for axisymmetric bodies in cylindrical tunnels. This extension has been already implemented by the author and will be reported elsewhere.

Appendix

Stream Function for a Source Ring in Unbounded Medium

The purpose of this appendix is to obtain the stream function due to a source ring kept in an unbounded medium. Employing the cylindrical coordinates (z, r) , let us consider a source ring of unit strength and radius r' with its center at $(z', 0)$ lying in a plane perpendicular to the z -axis. The incremental velocity potential at a point (z, r) due to an incremental arc of the ring is given by

$$d\phi = \frac{1}{4\pi} \frac{d\sigma}{[x^2 + r^2 + r'^2 - 2rr' \cos \gamma]^{\frac{3}{2}}}, \quad (\text{A-1})$$

where $x = |z - z'|$, γ is the included angle between the radius vectors r and r' and $d\sigma$ is the incremental source strength. Since the ring is of unit strength, $d\sigma = d\gamma/2\pi$ and the velocity potential is

$$\phi = \frac{1}{4\pi^2} \int_0^\pi \frac{d\gamma}{\sqrt{x^2 + R^2}}, \quad (\text{A-2})$$

where R^2 is defined by $R^2 = r^2 + r'^2 - 2rr' \cos \gamma$. The integrand in Equation (A-2) can be replaced by the infinite integral of Lipschitz [15] and the potential is then given by

$$\phi = \frac{1}{4\pi^2} \int_0^\pi d\gamma \int_0^\infty e^{-kx} J_0(kR) dk. \quad (\text{A-3})$$

By the application of Sonine-Gegenbaur integral [16], viz.

$$\frac{1}{\pi} \int_0^{\pi} J_0(kR) d\gamma = J_0(kr) J_0(kr') \quad (\text{A-4})$$

to Equation (A-3), the velocity potential can be rewritten as

$$\phi = \frac{1}{4\pi} \int_0^{\infty} e^{-kx} J_0(kr) J_0(kr') dk \quad (\text{A-5})$$

The stream function and the velocity potential are related by the well-known equations

$$\frac{\partial \phi}{\partial z} = \frac{1}{r} \frac{\partial \psi}{\partial r} \quad \text{and} \quad \frac{\partial \phi}{\partial r} = -\frac{1}{r} \frac{\partial \psi}{\partial z} \quad (\text{A-6})$$

Substituting the partial derivatives of ϕ obtained from Equation (A-5) into the Equations (A-6), and then integrating (A-6), we obtain

$$\psi = -\text{Sgn}(z - z') \frac{r}{4\pi} \int_0^{\infty} e^{-kx} J_1(kr) J_0(kr') dk + C \quad (\text{A-7})$$

where C is arbitrary constant, taken as zero henceforth, and Sgn is the Signum function defined by

$$\begin{aligned} \text{Sgn}(t) &= 1, \quad t \geq 0 \\ &= -1, \quad t < 0 \end{aligned} \quad (\text{A-8})$$

The product of the Bessel Functions, $J_1(kr) J_0(kr')$ in Equation (A-6) can be obtained by differentiating the Sonine-Gegenbaur integral, viz. Equation (A-4) with respect to r . Thus,

$$J_1(kr) J_0(kr') = \frac{1}{\pi} \int_0^\pi \frac{J_1(kR)}{R} (r - r' \cos \gamma) d\gamma \quad . \quad (A-9)$$

From Equations (A-7) and (A-9) we obtain

$$\psi = - \text{Sgn} (z - z') \frac{r}{4\pi^2} \int_0^\pi \frac{(r - r' \cos \gamma) d\gamma}{R} \int_0^\infty e^{-kx} J_1(kR) dk \quad . \quad (A-10)$$

The infinite integral with respect to the parameter k can be obtained from Hankel's generalization of the integral of Lipschitz [17]. The stream function is then given by

$$\psi = - \text{Sgn} (z - z') \frac{r}{4\pi^2} \int_0^\pi \frac{(r - r' \cos \gamma)}{R} \left(\frac{1}{R} - \frac{x}{R\sqrt{x^2 + R^2}} \right) d\gamma \quad . \quad (A-11)$$

It can be shown easily that the first integral,

$$\int_0^\pi \frac{(r - r' \cos \gamma) d\gamma}{R^2} = 0 \quad . \quad (A-12)$$

Substituting $\cos \gamma = 2 \cos^2 \frac{\gamma}{2} - 1$ in the second integral and changing the variable $\gamma = \pi - 2\theta$, we obtain, after some algebraic manipulations,

$$\psi = \text{Sgn} (z - z') \frac{x}{4\pi^2 p} \left[\frac{(r - r')}{(r + r')} \Pi (h, m) + K(m) \right] \quad , \quad (A-13)$$

where $p^2 = x^2 + (r + r')^2$, $\Pi (h, m)$ is the complete elliptic integral

of the third kind, defined as

$$\Pi(h, m) = \int_0^{\pi/2} \frac{d\theta}{(1 - h^2 \sin^2 \theta)(1 - m^2 \sin^2 \theta)^{\frac{1}{2}}} \quad , \quad (\text{A-14})$$

and $K(m)$ is the complete elliptic integral of the first kind, defined as

$$K(m) = \int_0^{\pi/2} \frac{d\theta}{(1 - m^2 \sin^2 \theta)^{\frac{1}{2}}} \quad . \quad (\text{A-15})$$

The parameters h and m are defined by

$$h^2 = \frac{4rr'}{(r + r')^2} \quad ; \quad m^2 = \frac{4rr'}{x^2 + (r + r')^2} \quad . \quad (\text{A-16})$$

In order to facilitate the computation of the stream function, Equation (A-13) is simplified further. It is observed that the condition $m^2 < h^2 < 1$ for $r \neq r'$, $z \neq z'$ corresponds to the circular case for the complete elliptic integral of the third kind [18]. Under this condition, the complete elliptic integral of the third kind can be expressed in terms of elliptic integrals of the first and the second kinds. We also define the related functions F_3 and F_3^* which are useful in our analysis as

$$F_3 = \text{Sgn}(z - z') F_3^* = 2\pi\psi \quad . \quad (\text{A-17})$$

From Equations (A-13), (A-17), and the results from Reference [18], it can be shown that

$$F_3^* = \frac{xr K(m)}{\pi p(r + r')} + \text{Sgn}(r - r') \frac{1}{4} [1 - \Lambda_0(\epsilon; m)] \quad . \quad (\text{A-18})$$

The function $\Lambda_0(\epsilon; m)$ of Equation (A-18) is the Heumann's Lambda function [19] given by

$$\Lambda_0(\epsilon; m) = \frac{2}{\pi} \left\{ K(m) E(\epsilon; m') - [K(m) - E(m)] F(\epsilon; m') \right\} , \quad (A-19)$$

where $F(\epsilon; m')$ and $E(\epsilon; m')$ respectively are the incomplete elliptic integrals of the first and the second kinds with parameter m' and amplitude ϵ . The parameters m' and m are complementary to each other and are related by

$$m^2 + m'^2 = 1 . \quad (A-20)$$

The amplitude ϵ is given by

$$\tan \epsilon = \frac{|r - r'|}{xm} . \quad (A-21)$$

It should be noted that for $z \neq z'$ and $r = r'$, $\Lambda_0(\epsilon; m) = 0$. Then the function F_3^* has a discontinuity of $1/2$ across $r = r'$. In order to ensure continuity of F_3^* across $r = r'$ we define

$$\left. \begin{aligned} F_3^* &= \frac{xrK(m)}{\pi p(r + r')} + \frac{1}{4} [1 - \Lambda_0(\epsilon; m)] , & r \geq r' \\ &= \frac{xrK(m)}{\pi p(r + r')} + \frac{1}{4} [1 + \Lambda_0(\epsilon; m)] , & r < r' \end{aligned} \right\} \quad (A-22)$$

The function F_3^* now becomes continuous for all values of z and r . But when $z = z'$, $r = r'$, $\Lambda_0(\epsilon; m) = 1$. Therefore, F_3 is continuous for all z and r except when $z = z'$, $r \leq r'$. For $r < r'$, $z \rightarrow z'_+$ we get $F_3 = 1/2$ while for $r < r'$, $z \rightarrow z'_-$ we have $F_3 = -1/2$. Thus the

function F_3 experiences a unit jump across the disc $z = z'$, $0 \leq r < r'$. Since the value of the stream function ψ at any point is equal to the volume of fluid passing between the streamline through the point and the reference streamline, this jump represents the volume of fluid issuing from the ring source. At the singular point $z = z'$, $r = r'$ the function F_3 becomes indeterminate. Approaching the singular point along a ray $|r - r'| = \tan \theta |z - z'|$, $-\pi/2 \leq \theta \leq \pi/2$, one observes that as $r \rightarrow r'$ and $z \rightarrow z'$, the amplitude $\epsilon \rightarrow |\theta|$. In this case

$$F_3 = \frac{1}{4} (1 - 2\theta/\pi) \quad , \quad z \rightarrow z'_+ \\ = -\frac{1}{4} (1 + 2\theta/\pi) \quad , \quad z \rightarrow z'_- .$$

(A-23)

Thus the value of F_3 at the singular point depends on the angle of approach. The foregoing results on the limiting values of F_3 are required in obtaining stream functions due to surface source distributions.

References

- [1] Bristow, D. R., "A Solution to the Inverse Problem for Incompressible, Axisymmetric Potential Flow," AIAA Paper 74-520, June 1974.
- [2] Zedan, M. F. and Dalton, C., "Incompressible Irrotational Axisymmetric Flow About a Body of Revolution: The Inverse Problem," Journal of Hydronautics, Vol. 12, January 1978, pp. 41-46.
- [3] Zedan, M. F. and Dalton, C., "Potential Flow Around Axisymmetric Bodies: Direct and Inverse Problems," AIAA Journal, Vol. 16, March 1978, pp. 242-250.
- [4] Young, A. D. and Owen, P. R., "A Simplified Theory for Streamline Bodies of Revolution, and its Application to the Development of High-Speed Low-Drag Shapes," R & M 2071, British Aeronautical Research Council, London, July 1943.
- [5] McNown, J. S., and Hsu, E. Y., "Approximation of Axisymmetric Body Forms for Specified Pressure Distributions," Journal of Applied Physics, Vol. 22, October 1951, pp. 874-867.
- [6] Marshall, F. J., "Design Problem in Hydrodynamics," Journal of Hydronautics, Vol. 4, October 1979, pp. 136-139.
- [7] Munzer, H. and Reichardt, H., "Axially Symmetric Source-Sink Bodies with Predominantly Constant Pressure Distributions," Rept. 6616, UM, 1944 (translated as TM 808-43 1959, U. S. Naval Ordnance Test Station, China Lake, California).
- [8] Garabedian, P. R., "An Example of Axially Symmetric Flow with a Free Surface," Studies in Mathematics and Mechanics Presented to Richard von Mises, Academic Press, New York, NY, 1954, pp. 149-159.

- [9] Jeppson, R. W., "Finite Difference Solutions to Free Jet and Confined Cavity Flows Past Disks with Preliminary Analyses of the Results," Utah Water Research Laboratory Report PRWG-76-1, Utah State University, Logan, Utah 84321, November 1969.
- [10] Hess, J. L. and James, R. M., "On the Problem of Shaping an Axisymmetric Body to Obtain Low Drag at Large Reynolds Number," McDonnell Douglas Report MDC J6791, 1975, Appendix A.
- [11] Hess, J. L., "Review of Integral-Equation Techniques for Solving Potential-Flow Problems with Emphasis on the Surface-Source Method," Computer Methods in Applied Mechanics and Engineering, Vol. 5, No. 2, March 1975.
- [12] Fernandez, J., "Flow Over an Axisymmetric Body in a Cylindrical Tunnel," ARL TM 79-31, March 1, 1979, The Pennsylvania State University, Institute for Science and Engineering, Applied Research Laboratory, State College, PA.
- [13] Smith, A. M. O., and Pierce, J., "Exact Solution of the Neumann Problem. Calculation of Non-Circulatory Plane and Axially Symmetric Flows about or within Arbitrary Boundaries," Douglas Aircraft Company, Inc., Report No. ES 26988, April 25, 1958.
- [14] Reinsch, C. H., "Smoothing by Spline Functions," Numerische Mathematik, Vol. 10, No. 3, 1967, pp. 177-183.
- [15] Watson, G. N., "A Treatise on the Theory of Bessel Functions," Cambridge University Press, 1944, Eq. (1), Section 13.2.
- [16] *ibid.*, Eqn. (16), Section 11.41.
- [17] *ibid.*, Eqn. (8), Section 13.2.

- [18] Abramovitz, M., and Stegun, I. A., ed. "Handbook of Mathematical Functions," National Bureau of Standards Applied Mathematics Series-55, June 1964, Eqn. (17.7.14), p. 559.
- [19] *ibid.*, Eqn. (17.4.40), p. 595.

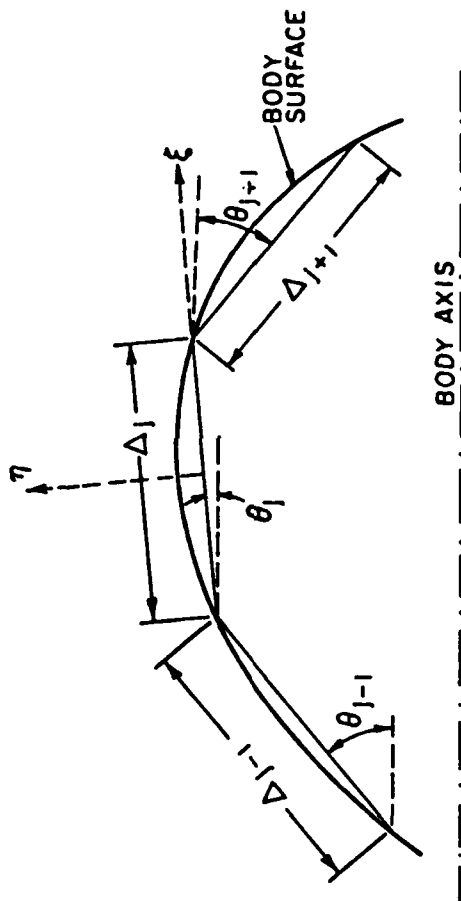


Figure 1. Element Geometry.

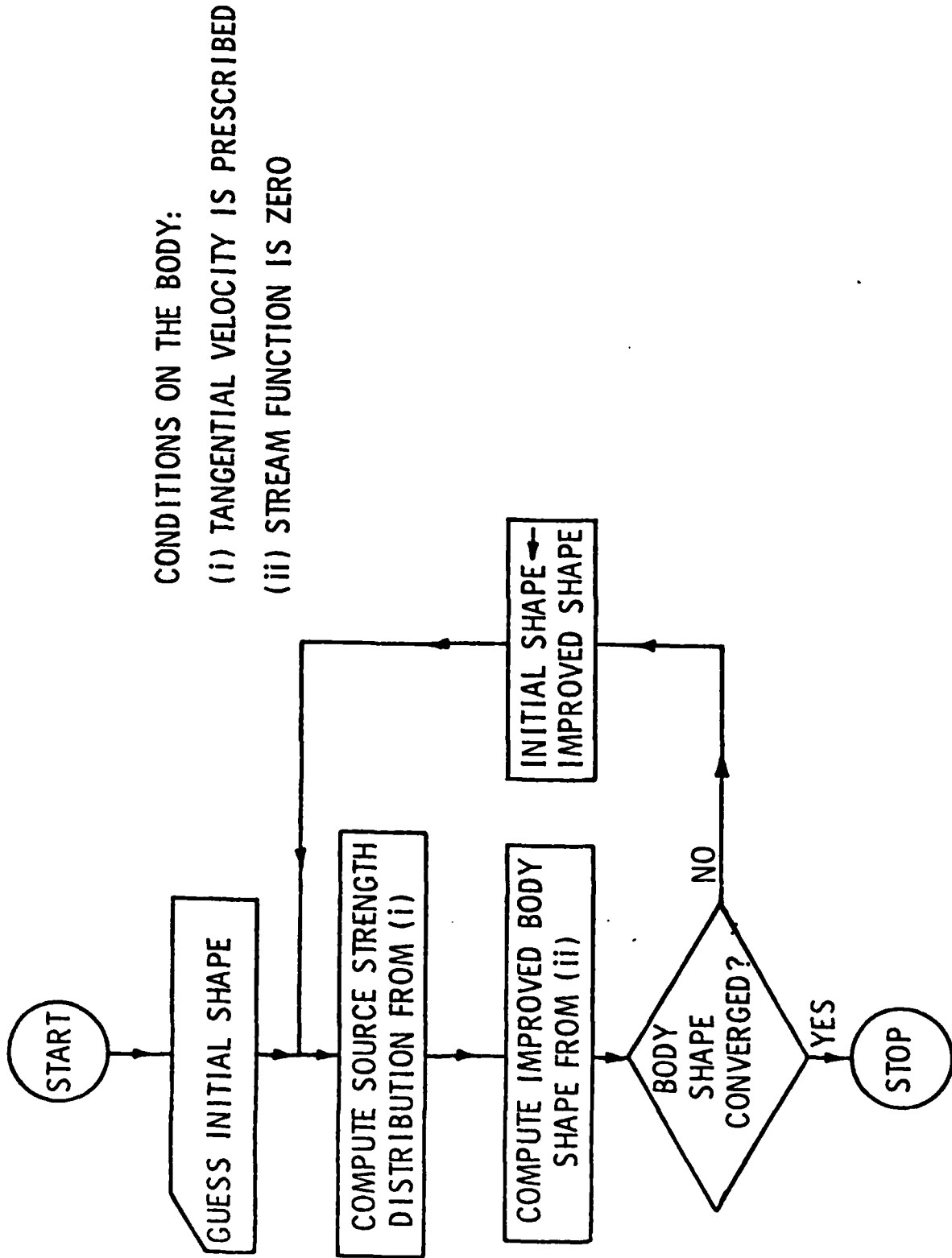


Figure 2. Algorithm for the Inverse Method.

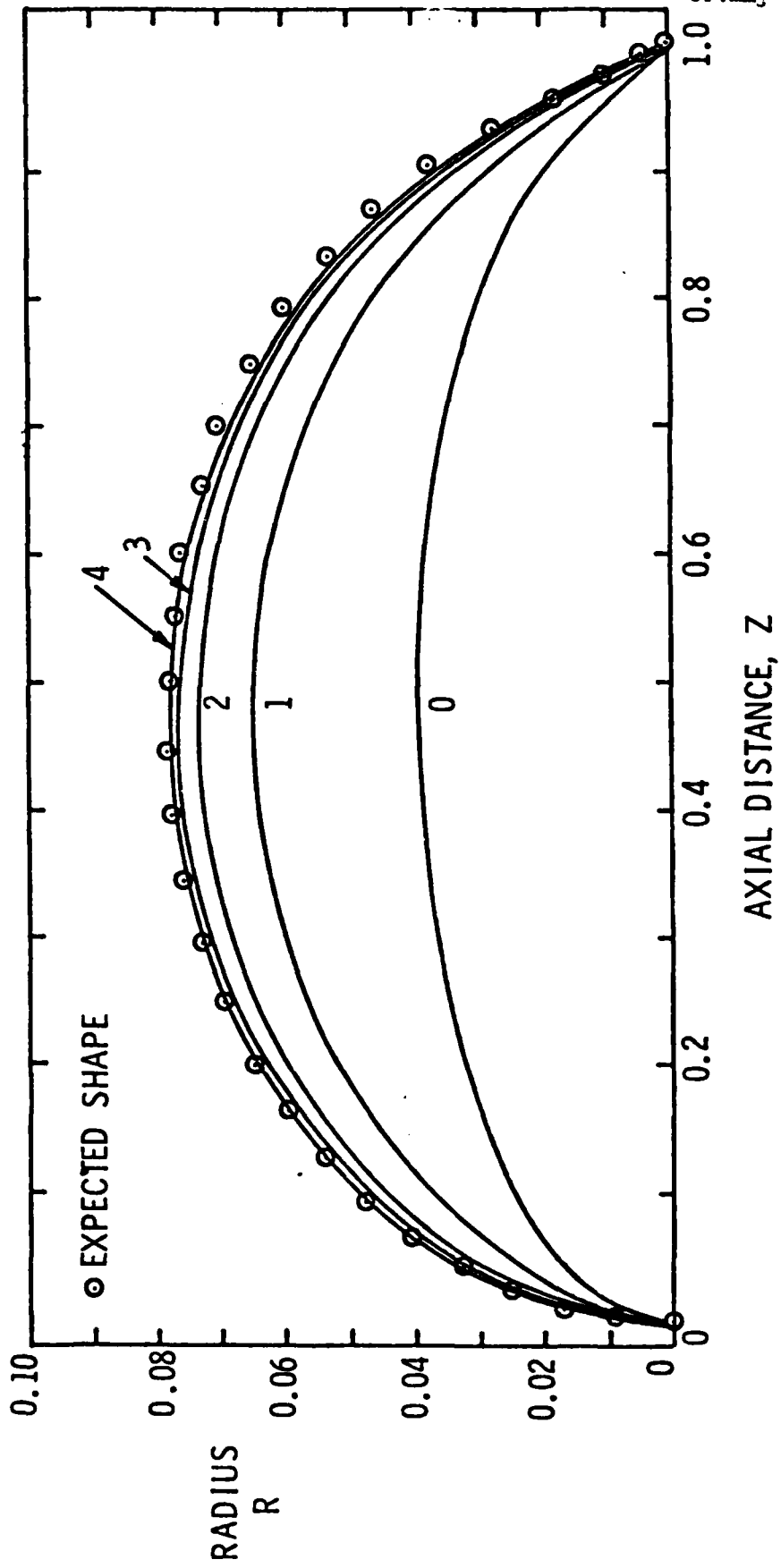


Figure 3. Successive Iterations for the Modified Spheroid.

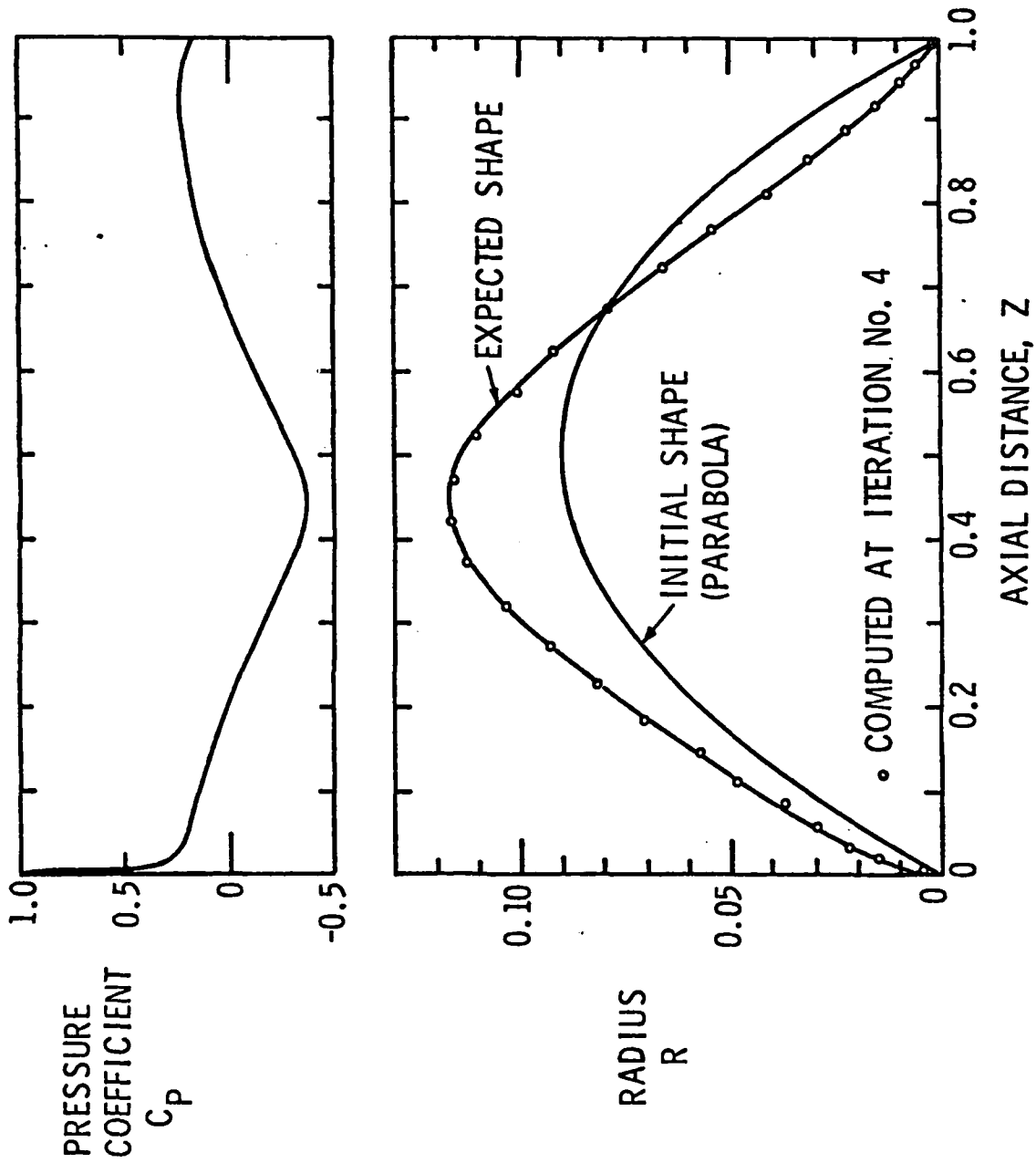


Figure 4. Low-Drag Cusped Body.

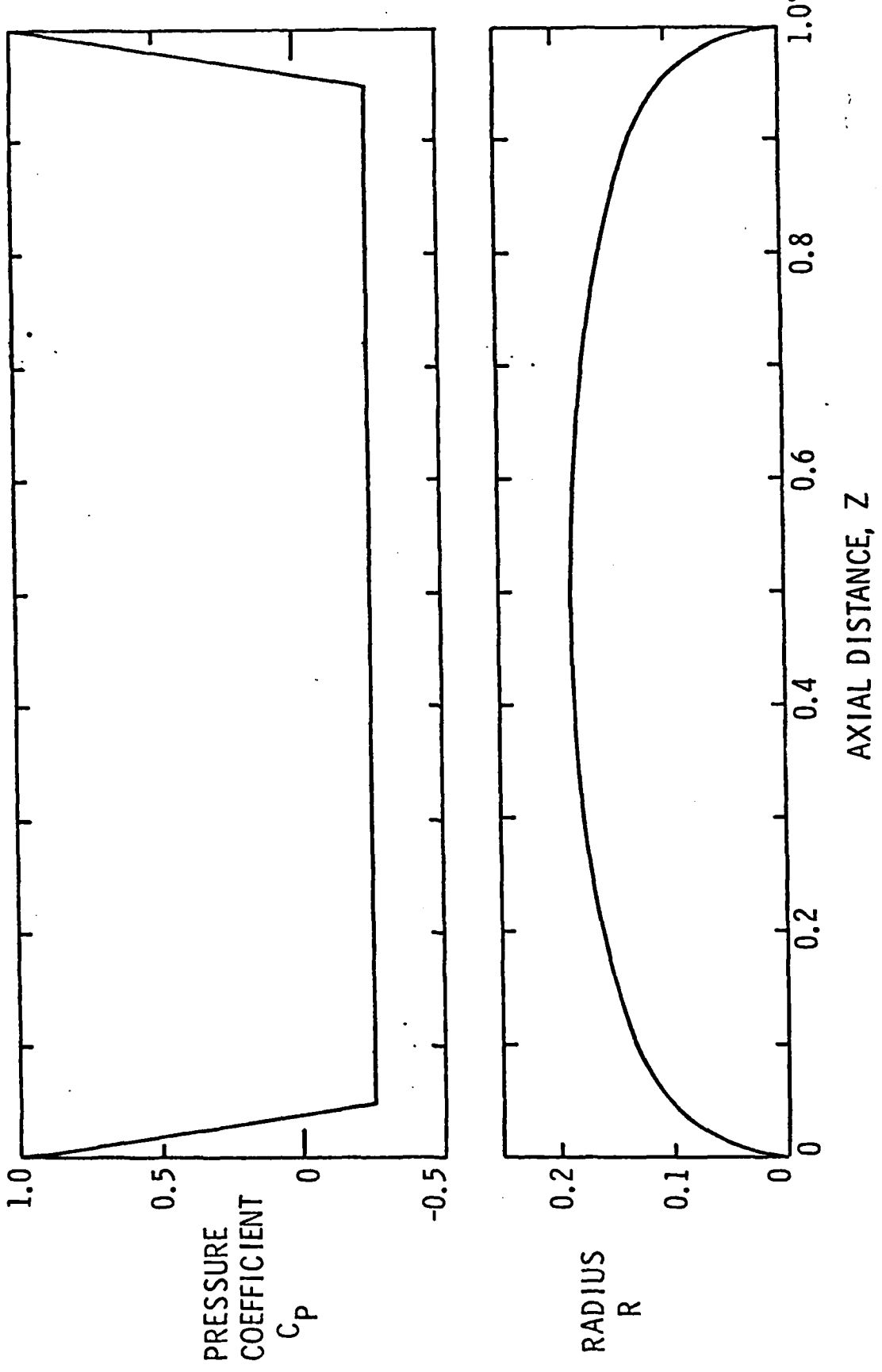


Figure 5. Roof-Top Pressure Distribution.

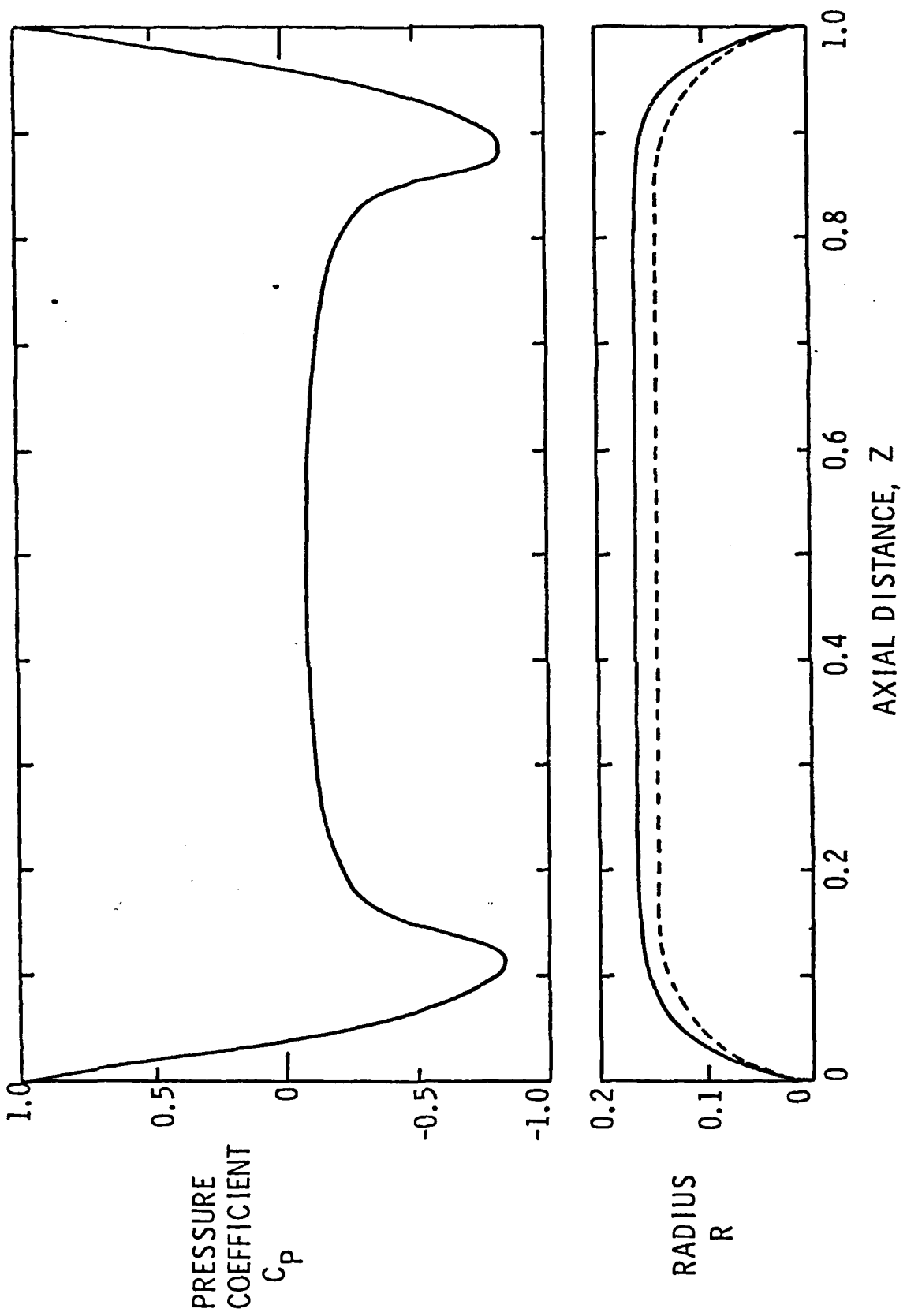


Figure 6. Equivalent Bodies

DISTRIBUTION LIST FOR UNCLASSIFIED TM 79-125 by J. Fernandez, dated June 25, 1979

Commander
Naval Sea Systems Command
Department of the Navy
Washington, DC 20362
Attn: Library
Code NSEA-09G32
(Copy No. 1 and 2)

Naval Sea Systems Command
Attn: H. C. Claybourne
Code NSEA-05H5
(Copy No. 3)

Naval Sea Systems Command
Attn: J. G. Juergens
Code NSEA-05H
(Copy No. 4)

Naval Sea Systems Command
Attn: E. G. Liszka
Code NSEA-63R1
(Copy No. 5)

Naval Sea Systems Command
Attn: C. G. McGuigan
Code NSEA-63R2
(Copy No. 6)

Naval Sea Systems Command
Attn: T. E. Peirce
Code NSEA-63R3
(Copy No. 7)

Naval Sea Systems Command
Attn: A. R. Paladino
Code NSEA-05H1
(Copy No. 8)

Naval Sea Systems Command
Attn: R. J. Cauley
Code NSEA-52B
(Copy No. 9)

Naval Sea Systems Command
Attn: W. L. Louis
Code NSEA-32132
(Copy No. 10)

Naval Sea Systems Command
Attn: F. J. Welling
Code NSEA-521
(Copy No. 11)

Commanding Officer
Naval Underwater Systems Center
Newport, RI 02840
Attn: Library
Code 54
(Copy No. 12)

Naval Underwater Systems Center
Attn: C. N. Pryor
Code 01
(Copy No. 13)

Commanding Officer
Naval Ocean Systems Center
San Diego, CA 92152
Attn: G. L. Donahue
Code 2542
(Copy No. 14)

Commanding Officer & Director
David W. Taylor Naval Ship R&D Center
Department of the Navy
Bethesda, MD 20084
Attn: Code 1505
(Copy No. 15)

David W. Taylor Naval Ship R&D Center
Attn: R. A. Cumming
Code 1544
(Copy No. 16)

David W. Taylor Naval Ship R&D Center
Attn: J. H. McCarthy
Code 1552
(Copy No. 17)

David W. Taylor Naval Ship R&D Center
Attn: M. M. Sevik
Code 19
(Copy No. 18)

David W. Taylor Naval Ship R&D Center
Attn: Y. T. Shen
Code 1524
(Copy No. 19)

Officer-In-Charge
David W. Taylor Naval Ship R&D Center
Department of the Navy
Annapolis Laboratory
Annapolis, MD 21402
Attn: J. G. Stricker
Code 2721
(Copy No. 20)

DISTRIBUTION LIST FOR UNCLASSIFIED TM 79-125 by J. Fernandez, dated June 25, 1979

Commanding Officer
Naval Undersea Warfare
Engineering Station
Department of the Navy
Keyport, WA 98345
(Copy No. 21)

Commanding Officer
Naval Ordnance Station
Louisville, KY 40214
(Copy No. 22)

Commander
Naval Surface Weapon Center
Silver Spring, MD 20910
Attn: G. C. Gaunard
Code R-31
(Copy No. 23)

Office of Naval Research
Department of the Navy
800 N. Quincy Street
Arlington, VA 22217
Attn: R. D. Cooper
Code 438
(Copy No. 24)

Office of Naval Research
Attn: H. Fitzpatrick
Code 438
(Copy No. 25)

Office of Naval Research
Attn: R. H. Imus
Code 102 IP
(Copy No. 26)

Defense Technical Information Center
5010 Duke Street
Cameron Station
Alexandria, VA 22314
(Copy No. 27 to and including 38)

Philadelphia Naval Shipyard
U. S. Naval Base
Philadelphia, PA 19112
Attn: F. Halpin
Code 260.6
(Copy No. 39)

National Bureau of Standards
Aerodynamics Section
Washington, DC 20234
Attn: P. S. Klebanoff
(Copy No. 40)

Naval Research Laboratory
Washington, DC 20390
Attn: R. J. Hansen
(Copy No. 41)

NASA Lewis Research Center
21000 Brookpark Road
Cleveland, Ohio 44135
Attn: J. Adamczyk
MS 5-9
(Copy No. 42)

Applied Physics Laboratory/
University of Washington (APL/UW)
1013 NE 40th Street
Seattle, WA 98105
(Copy No. 43)

Applied Research Laboratories/
University of Texas (ARL/UT)
Austin, Texas 78712
(Copy No. 44)

Dr. Bruce D. Cox
Stevens Institute of Technology
Davidson Laboratory
Castle Point Station
Hoboken, NJ 07030
(Copy No. 45)

California Institute of Technology
Jet Propulsion Laboratory
48000 Oak Grove Drive
Pasadena, CA 91109
Attn: Dr. L. Mack
(Copy No. 46)

Rand Corporation
1700 Main Street
Santa Monica, CA 90406
Attn: C. Gazley
(Copy No. 47)

Dr. Ir. A. De Bruijn
Technisch Physische Dienst TNO-TH
Stieltjesweg 1
Postbus 155
Delft
The Netherlands

Dr. John Foxwell
Admiralty Research Laboratory
Teddington, Middlesex
England
(Copy No. 49)

DISTRIBUTION LIST FOR UNCLASSIFIED TM 79-125 by J. Fernandez, dated June 25, 1979

Dr. D. G. Crighton
University of Leeds
Department of Applied
Mathematical Studies
Leeds LS29JT
England
(Copy No. 50)

Dr. Allan J. Acosta
California Institute of Technology
Division of Engineering for
Applied Sciences
Pasadena, CA 91109
(Copy No. 51)

Dynamics Technology, Inc.
3838 Carson Street, Suite 110
Torrance, CA 90503
Attn: Wayne H. Haigh
(Copy No. 52)

Bolt, Beranek and Newman
50 Moulton Street
Cambridge, MA 20136
Attn: Dr. N. A. Brown
(Copy No. 53)

Bolt, Beranek and Newman
Attn: D. Chase
(Copy No. 54)

Bolt, Beranek and Newman
Attn: K. L. Chandiramani
(Copy No. 55)

Professor Patrick Leehey - Rm. 5-222
Department of Ocean Engineering
Massachusetts Institute of Technology
77 Massachusetts Avenue
Cambridge, MA 02139
(Copy No. 56)

Dr. J. L. Lumley
Sibley School of Mechanical and
Aeronautical Engineering
Upson Hall
Cornell University
Ithaca, NY 14850
(Copy No. 57)

Calspan Corporation
4455 Genessee Street
Buffalo, NY 14221
Attn: Head Librarian
(Copy No. 58)

Naval Postgraduate School
The Presidio
Monterey, CA 93940
Attn: Library
(Copy No. 59)

Defense Advanced Research Projects Agency
1400 Wilson Boulevard
Arlington, VA 22209
Attn: P. Selwyn, TTO
(Copy No. 60)

Mr. E. M. Greitzer
MS-16 United Technologies
Research Center
Silver Lane
E. Hartford, CT 06118
(Copy No. 61)

Hydronautics, Inc.
Pindell School Road
Laurel, MD 20810
(Copy No. 62)

Dr. Douglas E. Humphreys
Naval Coastal Systems Center
Panama City, Florida 32407
(Copy No. 63)

Professor L. Landweber
Institute of Hydraulic Research
The University of Iowa
Iowa City, Iowa 52242
(Copy No. 64)

Dr. Charles Dalton
Mechanical Engineering Department
University of Houston
Houston, Texas 77004
(Copy No. 65)

Professor T. N. Krishnaswamy
Department of Aeronautics
Indian Institute of Science
Bangalore 56001
India
(Copy No. 66)

Mr. Dean R. Bristow
Dept. 241, Bldg. 32, L2
McDonnell Douglas Corporation
Box 516
Saint Louis, Missouri 63166
(Copy No. 67)

DISTRIBUTION LIST FOR UNCLASSIFIED TM 79-125 by J. Fernandez, dated June 25, 1979

Dr. A. M. O. Smith
Adjunct Professor
Energy and Kinetics Department
School of Engineering and
Applied Science
University of California
Los Angeles, CA 90024
(Copy No. 68)

Mr. John L. Hess
John L. Hess Associates
4338 Vista Street
Long Beach, CA 90803
(Copy No. 69)

Dr. Malcolm James
Aerodynamics and Research
Douglas Aircraft Company
Lakewood Boulevard
Long Beach, CA 90815
(Copy No. 70)

The Pennsylvania State University
Applied Research Laboratory
Post Office Box 30
State College, PA 16801
Attn: B. R. Parkin
(Copy No. 71)

Applied Research Laboratory
Attn: G. H. Hoffman
(Copy No. 72)

Applied Research Laboratory
Attn: G. C. Lauchle
(Copy No. 73)

Applied Research Laboratory
Attn: J. Fernandez
(Copy No. 74)

Applied Research Laboratory
Attn: Garfield Thomas Water Tunnel Files
(Copy No. 75)